Fast acoustic source imaging using multi-frequency sparse data

IOP Publishing Inverse Problems

Inverse Problems **36** (2020) 025009 (18pp) https://doi.org/10.1088/1361-6420/ab4aec

Fast acoustic source imaging using multi-frequency sparse data

Ala Alzaalig[1], Guanghui Hu[2], Xiaodong Liu[3] and Jiguang Sun[4]

[1] Department of Mathematical Sciences, Michigan Technological University
[2] Beijing Computational Science Research Center, Beijing 100193, People's Republic of China
[3] Institute of Applied Mathematics, Academy of Mathematics and Systems Science, Chinese Academy of Sciences, Beijing 100190, People's Republic of China
[4] Department of Mathematical Sciences, Michigan Technological University, Houghton, MI 49931, United States of America

E-mail: amalzaal@mtu.edu, hu@csrc.ac.cn, xdliu@amt.ac.cn and jiguangs@mtu.edu

Received 4 January 2019, revised 1 October 2019
Accepted for publication 4 October 2019
Published 23 January 2020

Abstract

We consider the acoustic source imaging problems in $\mathbb{R}^n$ using multiple frequency data at sparse directions/points. Using at most n observation directions/points, we show that the size and location of the source can be recovered. A non-iterative method is then proposed to image the source. The method is simple to implement and extremely fast since it only computes an indicator function on the domain of interest using matrix vector multiplications. Numerical examples are presented to validate the effectiveness of the method.

Keywords: acoustic source imaging, multi-frequency data, sampling method, uniqueness

(Some figures may appear in colour only in the online journal)

1. Introduction

Acoustic source imaging problems have attracted the attention of many researchers due to applications such as the pollution identification [7, 8], the localization [14] and determination of source current distribution in the brain [4].

In this paper, we consider the acoustic source imaging problem in a homogeneous background medium. Let $k = \omega/c > 0$ be the wave number of a time harmonic wave, where $\omega > 0$ and $c > 0$ denote the frequency and sound speed, respectively. Fixing a number $k_{\max} > 0$, we consider the reduced time-harmonic wave equation where the wave number is in an interval

$$k \in (0, k_{\max}). \tag{1.1}$$

Let

$$D := \bigcup_{m=1}^{M} D_m \subseteq \mathbb{R}^n$$

be an ensemble of finitely many bounded domains in $\mathbb{R}^n$, $n = 2, 3$, such that $\overline{D_j} \cap \overline{D_l} = \emptyset$ for $j \neq l$. Here $\overline{D}$ denotes the closure of D. In addition, we assume that $\mathbb{R}^n \backslash \overline{D}$ is connected. Let $F(\cdot, k) \in L^2(D), k \in (0, k_{\max})$ represent the acoustic source. It is usually obtained from the Fourier transform of a time-varying source. Denote by $H^1_{\text{loc}}(\mathbb{R}^n)$ the local Sobolev space of H^1 functions with compact support.

The time-harmonic wave $u \in H^1_{\text{loc}}(\mathbb{R}^n)$ radiated by F satisfies the inhomogeneous Helmholtz equation

$$\Delta u(x, k) + k^2 u(x, k) = F(x, k) \qquad \text{in } \mathbb{R}^n \tag{1.2}$$

and the Sommerfeld radiation condition

$$\lim_{r \longrightarrow \infty} r^{\frac{n-1}{2}} \left(\frac{\partial u}{\partial r} - \mathrm{i}ku \right) = 0, \qquad r = |x|. \tag{1.3}$$

From the Sommerfeld radiation condition (1.3), it is well known that the radiating field u has the following asymptotic behavior (see e.g. [3])

$$u(x, k) = C(k, n) \frac{\mathrm{e}^{\mathrm{i}k|x|}}{|x|^{\frac{n-1}{2}}} u^\infty(\theta_x, k) + \mathcal{O}(|x|^{-\frac{n+1}{2}}), \quad \theta_x = \frac{x}{|x|} \in S^{n-1},$$

as $r = |x| \longrightarrow \infty$, where S^{n-1} denotes the unit sphere in $\mathbb{R}^{n-1}$, $C(k, n) = \mathrm{e}^{\mathrm{i}\pi/4}/\sqrt{8\pi k}$ if $n = 2$ and $C(k, n) = 1/4\pi$ if $n = 3$. The complex valued function $u^\infty = u^\infty(\theta_x, k)$ is known as the far field pattern, where $\theta_x \in S^{n-1}$ is the observation direction.

The solution u to (1.2) and (1.3) has the form

$$u(x, k) = \int_D \Phi_k(x, y) F(y, k) \mathrm{d}s(y), \quad x \in \mathbb{R}^n, \tag{1.4}$$

with

$$\Phi_k(x, y) := \begin{cases} \frac{\mathrm{i}}{4} H_0^{(1)}(k|x - y|), & n = 2; \\ \frac{\mathrm{i}k}{4\pi} h_0^{(1)}(k|x - y|) = \frac{\mathrm{e}^{\mathrm{i}k|x-y|}}{4\pi|x-y|}, & n = 3, \end{cases}$$

being the fundamental solution of the Helmholtz equation. Here, $H_0^{(1)}$ and $h_0^{(1)}$ are Hankel function and spherical Hankel function of the first kind and order zero, respectively. From the asymptotic behavior of Hankel functions, we have that

$$u^\infty(\theta_x, k) = \int_D \mathrm{e}^{-\mathrm{i}k\theta_x \cdot y} F(y, k) \mathrm{d}y, \quad \theta_x \in S^{n-1}. \tag{1.5}$$

The multi-frequency inverse source problem (ISP) is to determine the source F from

- the radiating fields $u(x, k)$, $x \in \Gamma$, $k \in (0, k_{\max})$, where Γ is the measurement surface that contains D in its interior; or
- the far field patterns $u^\infty(\theta_x, k)$, $\theta_x \in S^{n-1}$, $k \in (0, k_{\max})$.

Most works in literature are devoted to recover the spatially-dependent source terms and assume that the data are measured at all observation spots, i.e. all $x \in \Gamma$ for the near field data or all $\theta_x \in S^{n-1}$ for the far field data. It is well known that a source with an extended support cannot be uniquely determined from measurements at a fixed frequency [5, 6]. Additional information on the source or the measurements are needed for the uniqueness [11, 12]. The use of the multiple frequency data for the ISPs provides an approach to obtain a unique solution to the inverse problems [1, 9]. In fact, it can be shown that the inverse problem is uniquely solvable and is even Lipschitz stable when $k_{\max}$ is larger than a certain real number [1]. Throughout this paper, we assume that the data are available for all $k \in (0, k_{\max})$.

In recent years, several reconstruction methods have been proposed to solve the multi-frequency ISPs. An iterative method with respect to frequencies is developed in [2]. In [16], the authors proposed a simple method based on the fact that the Fourier coefficients of the source can be obtained directly from the far field data. A factorization method in [10] reconstructs the support of the source with a limited set of far field data. In [15], Sylvester and Kelly produced a convex polygon containing the source. Note that the methods in [10, 15, 16] require that the source is independent of the frequency.

In this work, we consider a frequency dependent source F, which corresponds to the time dependent source in the time domain problems. For the case of near field measurements, we assume that u is measured at finitely many points,

$$\{x_1, x_2, \cdots, x_M\} =: \Gamma_M \subset \Gamma.$$

Accordingly, we obtain the following broadband sparse near field measurements

$$\{u(x_m, k) \,|\, x_m \in \Gamma_M,\ k \in (0, k_{\max})\}. \tag{1.6}$$

For the case of far field measurements, we suppose that the far field data is measured in finitely many observation directions,

$$\{\theta_1, \theta_2, \cdots, \theta_M\} =: \Theta_M \subset S^{n-1}.$$

Consequently, we obtain the following broadband sparse far field measurements

$$\{u^\infty(\theta_m, k) \,|\, \theta_m \in \Theta_M,\ k \in (0, k_{\max})\}. \tag{1.7}$$

The inverse problem we are interested is to reconstruct the support of the source F from the data defined in (1.6) or (1.7). It is impossible to uniquely determine the source (see the counter example (2.11) and (2.12) in section 2.1). Nevertheless, we will show that partial information of the source, e.g. the location and the support, can be obtained. The first contribution of this paper is the analysis of the inverse problem when the source depends on the wave number. The second contribution of this paper is a novel sampling method. If the far field data are available in a single observation direction, we construct an indicator function which provides a strip containing the source. Far field data of two linearly independent observation directions give a rough reconstruction for the support of the source. The method is simple to implement and very fast since main task is to evaluate some integrals numerically.

The rest of this paper is arranged as follows. Some uniqueness results will be established in section 2 using multi-frequency data at a single measurement point. Section 3 is devoted to a novel indicator function using complete far field data. It is shown that the indicator decays as Bessel functions from the source. In section 4, we consider the case when the far field data can be measured at finitely many observation directions. In particular, the behavior of the indicator for a single observation direction is studied. Section 5 contains several numerical examples in two dimensions to demonstrate the performance of the proposed method.

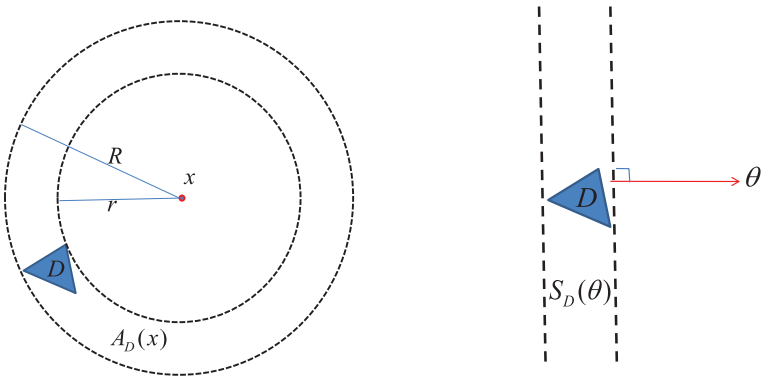

Figure 1. One object in $\mathbb{R}^2$. Left: the smallest annular $A_D(x)$ with center at the measurement point x; Right: the smallest strip $S_D(\theta)$ with normal in the observation direction θ.

2. Uniqueness results from multi-frequency data at a single measurement point

This section is devoted to the study of what information can be obtained using multi-frequency data at a single measurement point. Specifically, the measurements are either the broadband near field data $u(x,k)$, $k \in (0,k_{\max})$ at a fixed measurement point $x \in \Gamma_M$, or the broadband far field data $u^\infty(\theta,k), k \in (0,k_{\max})$ for a single observation direction $\theta \in \Theta_M$. For a bounded domain D, the x-annular hull for $x \in \Gamma_M$ is defined by

$$A_D(x) := \{y \in \mathbb{R}^n \mid \inf_{z\in D} |x-z| \leqslant |x-y| \leqslant \sup_{z\in D} |x-z|\}$$

and the θ-strip hull of D for $\theta \in \Theta_M$ is defined by

$$S_D(\theta) := \{y \in \mathbb{R}^n \mid \inf_{z\in D} z\cdot\theta \leqslant y\cdot\theta \leqslant \sup_{z\in D} z\cdot\theta\}.$$

See figure 1 for these two hulls in two dimensions.

We assume that the source $F(x,k)$ takes one of the following forms:

- $F(x,k) = f(x)g(k)$, where $g \in \mathcal{C}(0,k_{\max})$, a continuous function on $(0,k_{\max})$;
- $F(x,k) = f(x)\frac{e^{ik|x-z|}}{4\pi|x-z|}$, $z \in \mathbb{R}^3\backslash\overline{D}$;
- $F(x,k) = f(x)e^{ikx\cdot d}$, $d \in S^{n-1}$.

The last two cases also arise in the Born approximation for scattering problems of an inhomogeneous medium. The mathematical model is

$$\Delta u^t + k^2 q u^t = 0.$$

The total field u^t is of the form $u^t = u^i + u^s$, where the incident wave u^i is a solution to the homogeneous Helmholtz equation and the scattered wave u^s is the radiating solution to

$$\Delta u^s + k^2 u^s = k^2(1-q)(u^i + u^s). \tag{2.1}$$

The incident wave u^i is either a plane wave $e^{ikx\cdot\theta}$, $\theta \in S^{n-1}$, or a point source $\frac{e^{ik|x-z|}}{4\pi|x-z|}, x \neq z$. When u^s is small enough to be ignored on the right hand side of (2.1), the Born approximation u_B to u^s is such that

$$\Delta u_B + k^2 u_B = k^2(1-q)u^i. \tag{2.2}$$

Dividing (2.2) by k^2, the right hand side of (2.2) reduces to the last two cases of $F(x,k)$ for different incident waves.

2.1. $F(x,k) = f(x)g(k), g \in \mathcal{C}(0,k_{\max})$

First, consider the case when the source $F(x,k)$ is a product of a spatial function f and a frequency function g. Here, $g \in \mathcal{C}(0,k_{\max})$ is a given nontrivial function of k. Then there exists an interval $I := (a,b) \subset (0,k_{\max})$ such that

$$g(k) \neq 0, \quad k \in I \subset (0,k_{\max}). \tag{2.3}$$

For the near field case in $\mathbb{R}^3$, we assume that $u(x,k)$ is measured for all $k \in I$ at a fixed point $x \in \mathbb{R}^3 \backslash \overline{D}$. Let $S_r(x)$ be the sphere centered at x with radius r. Using (1.4), we obtain that

$$v(x,k) := \frac{u(x,k)}{g(k)} = \int_{\mathbb{R}^3} f(y) \frac{\mathrm{e}^{\mathrm{i}k|x-y|}}{4\pi|x-y|} \mathrm{d}y = \int_{-\infty}^{\infty} \widetilde{f}(r)\mathrm{e}^{\mathrm{i}kr}\mathrm{d}r, \quad k \in I, \tag{2.4}$$

where

$$\widetilde{f}(r) := \begin{cases} \frac{1}{4\pi r}\int_{S_r(x)} f(y)\mathrm{d}s(y), & r > 0; \\ 0, & r \leqslant 0. \end{cases} \tag{2.5}$$

The following theorem shows that multi-frequency data determine a unique annular containing the support of the target.

Theorem 2.1. *Assume that $F(x,k) = f(x)g(k)$, where g is a given continuous function satisfying (2.3), and that the set*

$$\{r \in (0,\infty) |\, S_r(x) \subset A_D(x), \widetilde{f}(r) = 0\} \tag{2.6}$$

has Lebesgue measure zero. Then, the annular $A_D(x)$ can be uniquely determined by the scattered field $u(x,k)$ for all $k \in I$ at a fixed point $x \in \mathbb{R}^3 \backslash \overline{D}$.

Proof. Due to (2.4), $v(x,k)$ is an analytic function of the wave number k. It is clear from (2.4) that $v(x,k)$ is the inverse Fourier transform of $\widetilde{f}$. Thus $\widetilde{f}$ is uniquely determined by the measurements $u(x,k)$ for all $k \in I$ at a fixed point $x \in \mathbb{R}^3 \backslash \overline{D}$. Since the set in (2.6) has Legesgue measure zero, we have

$$A_D(x) = \overline{\bigcup_{r \in (0,\infty)} \{S_r(x) | \widetilde{f}(r) \neq 0\}},$$

which implies that the annular $A_D(x)$ is uniquely determined by $\widetilde{f}$, and also by $u(x,k)$ for all $k \in I$, at a fixed point $x \in \mathbb{R}^3 \backslash \overline{D}$. The proof is complete. □

The equality (2.4) takes the form of Fourier transform, and therefore plays an important role in the proof. However, this does not hold in $\mathbb{R}^2$ due to the fundamental solution of the Helmholtz equation.

Now we turn to the far field measurements $u^\infty(\theta,k)$ for all $k \in (0,k_{\max})$, at a fixed observation direction $\theta \in S^{n-1}$. Let

$$\Pi_\tau := \{y \in \mathbb{R}^n | y \cdot \theta + \tau = 0\}$$

be a hyperplane with normal direction θ. From (1.5), by noting again that $g(k) \neq 0$ for $k \in I$, we have

$$v^{\infty}(\theta, k) := \frac{u^{\infty}(\theta, k)}{g(k)} = \int_{\mathbb{R}^n} \mathrm{e}^{-\mathrm{i}k\theta \cdot y} f(y) \mathrm{d}y = \int_{\mathbb{R}} \hat{f}(\tau) \mathrm{e}^{\mathrm{i}k\tau} d\tau, \ \theta \in S^{n-1}, \quad (2.7)$$

where

$$\hat{f}(\tau) := \int_{\Pi_\tau} f(y) \mathrm{d}s(y). \quad (2.8)$$

The analogous result of Theorem 2.1 for the far field measurements is formulated in the following theorem.

Theorem 2.2. *Assume $F(x,k) = f(x)g(k)$ with a given continuous function g satisfying (2.3). If the set*

$$\{\tau \in \mathbb{R} | \, \Pi_\tau \subset S_D(\theta), \hat{f}(\tau) = 0\} \quad (2.9)$$

has Lebesgue measure zero, then the strip $S_D(\theta)$ can be uniquely determined by the far field measurements $u^{\infty}(\theta, k)$ for all $k \in I$, at a fixed observation direction $\theta \in S^{n-1}$.

The proof of theorem 2.2 is similar to that of theorem 2.1. However, the uniqueness result using far field measurements holds both in two and three dimensions.

Finally, we give some remarks on the assumptions on the sets in (2.6) and (2.9).

- The sets in (2.6) and (2.9) have Lebesgue measure zero if the real part of a complex multiple of the spatial function f is bounded away from zero on their support, i.e. we assume that $f \in L^{\infty}(D)$ is such that there exist $\alpha \in \mathbb{R}$ and $c_0 > 0$ such that

$$\Re(\mathrm{e}^{\mathrm{i}\alpha} f(x)) \geqslant c_0, \quad \text{a.e. in } D. \quad (2.10)$$

- Theorems 2.1 and 2.2 are not true in general if the sets in (2.6) and (2.9), respectively, have positive Lebesgue measure. For example, for $x = (x_1, x_2) \in \mathbb{R}^2$, consider

$$f_1(x) = \begin{cases} 1, & x_1 \in (-1,1), x_2 \in [1,2); \\ x_1, & x_1 \in (-1,1), x_2 \in (-1,1); \\ 1, & x_1 \in (-1,1), x_2 \in (-2,-1]; \\ 0, & \text{otherwise}, \end{cases} \quad (2.11)$$

and

$$f_2(x) = \begin{cases} 1, & x_1 \in (-1,1), x_2 \in [1,2); \\ 1, & x_1 \in (-1,1), x_2 \in (-2,-1]; \\ 0, & \text{otherwise}. \end{cases} \quad (2.12)$$

Then $f_1 \in L^2(\mathbb{R}^2)$ with compact support in $D_1 = [-1,1] \times [-2,2]$, and $f_2 \in L^2(\mathbb{R}^2)$ with compact support in $D_2 := D_2^{(1)} \cup D_2^{(2)}$, where $D_2^{(1)} = [-1,1] \times [-2,-1]$ and $D_2^{(2)} = [-1,1] \times [1,2]$. A straightforward calculation shows that the far field patterns corresponding to these two different sources coincide for all wave numbers at the fixed observation direction $\theta = (0,1)$. We also refer to figure 9 for the numerical result.

2.2. $F(x,k) = f(x)\frac{e^{ik|x-z|}}{4\pi|x-z|}, z \in \mathbb{R}^3\backslash\overline{D}$

We consider the second case, i.e. the source F takes the form

$$F(x,k) = f(x)\frac{e^{ik|x-z|}}{4\pi|x-z|}, \quad x \in \mathbb{R}^3\backslash\{z\}, z \in \mathbb{R}^3\backslash\overline{D}.$$

Let $S'_r(x,z) := \{y \in \mathbb{R}^3 |\ |x-y| + |y-z| = r\}$ be an ellipsoid and $A'_D(x,z)$ be the smallest annular-like domain (the difference of two ellipsoids) containing D. Recalling (1.4), we have that

$$u(x,k) = \int_{\mathbb{R}^3} f(y)\frac{e^{ik(|x-y|+|y-z|)}}{(4\pi)^2|x-y|\,|z-y|}dy = \int_{\mathbb{R}} \widetilde{f}'(r)e^{ikr}dr, \quad k \in I, \tag{2.13}$$

where

$$\widetilde{f}'(r) := \begin{cases} \int_{S'_r(x,z)} \frac{f(y)}{(4\pi)^2|x-y||z-y|}ds(y), & r > |x-z|; \\ 0, & r \leqslant |x-z|. \end{cases} \tag{2.14}$$

Similar to the case considered in theorem 2.1, we have the following uniqueness result.

Theorem 2.3. *Assume $F(x,k) = f(x)\frac{e^{ik|x-z|}}{4\pi|x-z|}$ for a given point $z \in \mathbb{R}^3\backslash\overline{D}$. If the set*

$$\{r \in (0,\infty)|\ S'_r(x,z) \subset A'_D(x,z), \widetilde{f}'(r) = 0\} \tag{2.15}$$

has Lebesgue measure zero. Then the annular-like domain $A'_D(x,z)$ can be uniquely determined by $u(x,k)$ for all $k \in (0,k_{\max})$ at a fixed point $x \in \mathbb{R}^3\backslash\overline{D}$, $x \neq z$.

2.3. $F(x,k) = f(x)e^{ikx\cdot d}, d \in S^{n-1}$

Consider now the case when $F(x,k) = f(x)e^{ikx\cdot d}$ with a given direction $d \in S^{n-1}$. Using (1.5) again, we have that, for $\theta \neq d$,

$$u^\infty(\theta,k) = \int_{\mathbb{R}^n} e^{-ik(\theta-d)\cdot y}f(y)dy, \quad d,\theta \in S^{n-1},\ k \in (0,k_{\max}). \tag{2.16}$$

Define $\theta_d := (\theta-d)/|\theta-d| \in S^{n-1}$. The inverse problem is equivalent to seek $F(x,k) = f(x)$ from the far field measurements $u^\infty(\theta_d,k)$ for all $k \in (0,k_{\max}|\theta-d|)$. From theorem 2.2, we have the following uniqueness result.

Theorem 2.4. *Assume $F(x,k) = f(x)e^{ikx\cdot d}$ with a given direction $d \in S^{n-1}$. If the set*

$$\{\tau \in \mathbb{R}|\ \Pi_\tau \subset S_D(\theta_d), \hat{f}(\tau) = 0\} \tag{2.17}$$

has Lebesgue measure zero, then the strip $S_D(\theta_d)$ can be uniquely determined by the far field measurements $u^\infty(\theta,k)$ for all $k \in (0,k_{\max})$ at a fixed observation direction $\theta \in S^{n-1}$.

3. A novel source indicator function

We begin with the ISP using the far field patterns $u^\infty(\theta_x,k)$ for all observation directions $\theta_x \in S^{n-1}$ and all wave numbers $k \in (0,k_{\max})$. To reconstruct the support of a general source $F(x,k)$, we introduce the function

$$I(z) = \left| \int_0^{k_{\max}} \int_{S^{n-1}} u^\infty(\theta_x, k)\, \mathrm{e}^{\mathrm{i}k\theta_x \cdot z} \mathrm{d}s(\theta_x)\, \mathrm{d}k \right|, \tag{3.1}$$

where $z \in \mathbb{R}^n$ is called the sampling point. As will be seen later, the above function gives partial information (size and location) of the source and is thus referred to as the source *indicator* function. Note that no *a priori* information on the source is required and the source indicator function is simple to compute since only integral evaluations are needed. Furthermore, we will show later that the source indicator function continuously depends on the noise in the data.

Inserting (1.5) into (3.1), changing the order of the integration, and using the Funk–Hecke formula [13], we deduce that

$$\begin{aligned} I(z) &= \left| \int_0^{k_{\max}} \int_{S^{n-1}} u^\infty(\theta_x, k)\, \mathrm{e}^{\mathrm{i}k\theta_x \cdot z} \mathrm{d}s(\theta_x)\, \mathrm{d}k \right| \\ &= \left| \int_0^{k_{\max}} \int_{S^{n-1}} \int_D \mathrm{e}^{-\mathrm{i}k\theta_x \cdot y} F(y,k) \mathrm{d}y\, \mathrm{e}^{\mathrm{i}k\theta_x \cdot z} \mathrm{d}s(\theta_x)\, \mathrm{d}k \right| \\ &= \left| \int_0^{k_{\max}} \int_D \int_{S^{n-1}} \mathrm{e}^{-\mathrm{i}k\theta_x \cdot y}\, \mathrm{e}^{\mathrm{i}k\theta_x \cdot z} \mathrm{d}s(\theta_x)\, F(y,k) \mathrm{d}y\, \mathrm{d}k \right| \\ &= \left| \int_0^{k_{\max}} \mu \int_D g(k|y-z|) F(y,k) \mathrm{d}y\, \mathrm{d}k \right|, \end{aligned} \tag{3.2}$$

where

$$\mu = \begin{cases} 2\pi, & n = 2; \\ 4\pi, & n = 3, \end{cases} \quad \text{and} \quad g(t) = \begin{cases} J_0(t), & n = 2; \\ j_0(t), & n = 3. \end{cases} \tag{3.3}$$

Here, J_0 and j_0 are the Bessel function and spherical Bessel function of order zero, respectively. This implies that the source indicator function $I(z)$ is a superposition of the Bessel functions in 2D or spherical Bessel functions in 3D. We have the following asymptotic formulas for the Bessel and spherical Bessel functions (see figure 2)

$$\begin{aligned} J_0(t) &= \frac{\sin t + \cos t}{\sqrt{\pi t}} \left\{ 1 + O\Big(\frac{1}{t}\Big) \right\}, \text{ as } t \to \infty, \\ j_0(t) &= \frac{\sin t}{t} \left\{ 1 + O\Big(\frac{1}{t}\Big) \right\}, \text{ as } t \to \infty. \end{aligned}$$

Thus, we expect that the source indicator function I_z decays as the Bessel functions when the sampling point z moves away from the support D.

We end this section by a stability statement, which states that the indicator depends on the noise continuously.

Theorem 3.1 (Stability). *Let u_δ^∞ be the measured far field pattern with noises. Then*

$$|I(z) - I_\delta(z)| \leqslant \mu \int_0^{k_{\max}} \left\| u^\infty(\cdot, k) - u_\delta^\infty(\cdot, k) \right\|_{L^2(S^{n-1})} \mathrm{d}k, \tag{3.4}$$

where $I_\delta(z)$ is the source indicator function with u^∞ replaced by u_δ^∞, μ is a constant given by (3.3).

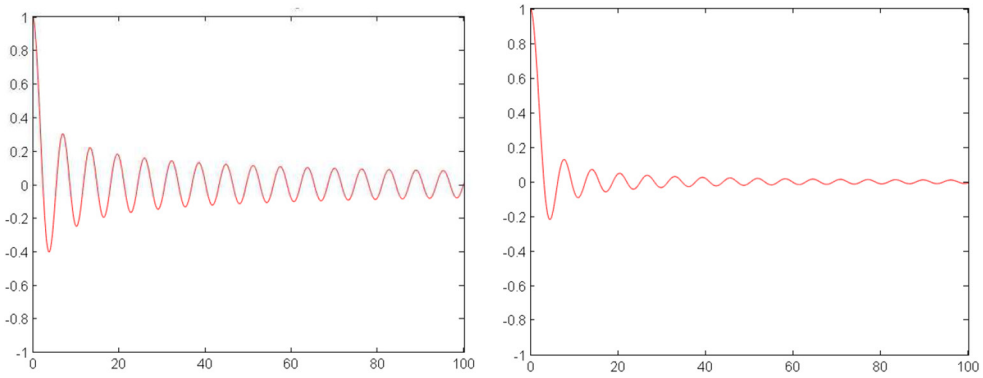

Figure 2. Decay behavior of the Bessel function J_0 (Left) and the spherical Bessel function j_0 (Right) .

Proof.

$$
\begin{aligned}
&I(z) - I_\delta(z) \\
&:= \Big| \int_0^{k_{\max}} \int_{S^{n-1}} u^\infty(\theta_x, k) \mathrm{e}^{\mathrm{i}k\theta_x \cdot z} \mathrm{d}s(\theta_x) \mathrm{d}k \Big| \\
&\qquad - \Big| \int_0^{k_{\max}} \int_{S^{n-1}} u_\delta^\infty(\theta_x, k) \mathrm{e}^{\mathrm{i}k\theta_x \cdot z} \mathrm{d}s(\theta_x) \mathrm{d}k \Big| \\
&\leqslant \int_0^{k_{\max}} \int_{S^{n-1}} \Big| [u^\infty(\theta_x, k) - u_\delta^\infty(\theta_x, k)] \mathrm{e}^{\mathrm{i}k\theta_x \cdot z} \Big| \mathrm{d}s(\theta_x) \mathrm{d}k \\
&\leqslant \mu \int_0^{k_{\max}} \Big\| u^\infty(\cdot, k) - u_\delta^\infty(\cdot, k) \Big\|_{L^2(S^{n-1})} \mathrm{d}k,
\end{aligned}
$$

where we have used the triangle inequality and the Cauchy–Schwarz inequality. □

4. Multi-frequency ISPs

This section is devoted to an inversion scheme that utilizes multi-frequency sparse measurements to reduce the full-aperture data required in the previous section. Our aim is to image the position and support of some frequency-dependent sources.

For a single observation direction $\theta_m \in \Theta_M$, we introduce the following source indicator function

$$
I^{\theta_m}(z) = \Big| \int_0^{k_{\max}} u^\infty(\theta_m, k) \mathrm{e}^{\mathrm{i}k\theta_m \cdot z} \mathrm{d}k \Big|. \tag{4.1}
$$

For all the available observation directions in Θ_M, we define

$$
I^{\Theta_M}(z) := \sum_{\theta_m \in \Theta_M} I^{\theta_m}(z). \tag{4.2}
$$

We begin with the behavior of the source indicator function I^{θ_m}, which uses the multi-frequency far field patterns $u^\infty(\theta_m, k)$ with a single observation direction $\theta_m \in S^{n-1}$. Let $\theta_m^\perp$ be a direction perpendicular to θ_m and we have

$$I^{\theta_m}(z+\alpha\theta_m^{\perp}) = I^{\theta_m}(z), \quad \forall z \in \mathbb{R}^n,\ \alpha \geqslant 0, \tag{4.3}$$

since $\theta_m^{\perp} \cdot \theta_m = 0$. This implies that the source indicator function I^{θ_m} has the same value for sampling points in the hyperplane with normal direction θ_m.

In the following, we assume that the source F depends smoothly on the wave number k, say $\mathcal{C}^1$. Recall from (1.5) that the far field pattern has the following representation

$$u^{\infty}(\theta_m, k) = \int_D \mathrm{e}^{-\mathrm{i}k\theta_m \cdot y} f(y,k)\mathrm{d}y, \quad \theta_m \in \Theta_M,\ k \in (0, k_{\max}).$$

Inserting it into the source indicator function I^{θ_m} defined in (4.1), changing the order of integration, and integrating by parts, we have

$$\begin{aligned} I^{\theta_m}(z) &= \left| \int_D \int_0^{k_{\max}} \mathrm{e}^{\mathrm{i}k\theta_m \cdot (z-y)} F(y,k)\mathrm{d}k\mathrm{d}y \right| \\ &= \left| \int_D \frac{\mathcal{F}_z(y)}{\theta_m \cdot (z-y)} \mathrm{d}y \right|, \end{aligned} \tag{4.4}$$

where the numerator $\mathcal{F}_z(y) \in L^{\infty}(D)$ is given by

$$\mathcal{F}_z(y) := \mathrm{e}^{\mathrm{i}k_{\max}\theta_m \cdot (z-y)} F(y, k_{\max}) - F(y,0) - \int_0^{k_{\max}} \mathrm{e}^{\mathrm{i}k\theta_m \cdot (z-y)} \frac{\partial F}{\partial k}(y,k)\mathrm{d}k,\ y \in D.$$

It is clear that the source indicator function I^{θ_m} is a superposition of functions that decay as $1/|\theta_m \cdot (z-y)|$ as the sampling point z goes away from the strip $S_D(\theta_m)$.

In conclusion, the values of the source indicator function I^{θ_m} remain invariant on the hyperplane with the normal direction θ_m, and decay as the sampling point z moves away from the strip $S_D(\theta_m)$. Therefore, a strip $S_D(\theta_m)$ can be reconstructed using I^{θ_m}. A natural idea is to use the source indicator function I^{Θ_M} given in (4.2) to construct the so called Θ_M-convex hull of D [15]

$$S_D(\Theta_M) := \bigcap_{\theta_m \in \Theta_M} S_D(\theta_m).$$

5. Numerical examples

Now we present some examples to demonstrate the indicators proposed in the previous section in two dimensions using multiple frequency far field data. The synthetic data of the forward problems are computed using (1.5). Let D be the compact support of F. We generate a triangular mesh $\mathcal{T}$ for D with mesh size $h \approx 0.01$. For the direction

$$\theta := (\cos\varphi, \sin\varphi)$$

and fixed k, the far-field pattern is approximated by

$$u^{\infty}(\theta; k) \approx \sum_{T \in \mathcal{T}} \mathrm{e}^{-\mathrm{i}k\theta \cdot y_T} f(y_T)|T|, \tag{5.1}$$

where $T \in \mathcal{T}$ is a triangle, y_T is the center of T, and $|T|$ denotes the area of T. The simulated far-field data contain less than 2% numerical error.

In all examples, for $\theta_m \in \Theta_M$, one has the far field data

$$u^{\infty}(\theta_m; k_j), \quad j = 1, \ldots N,$$

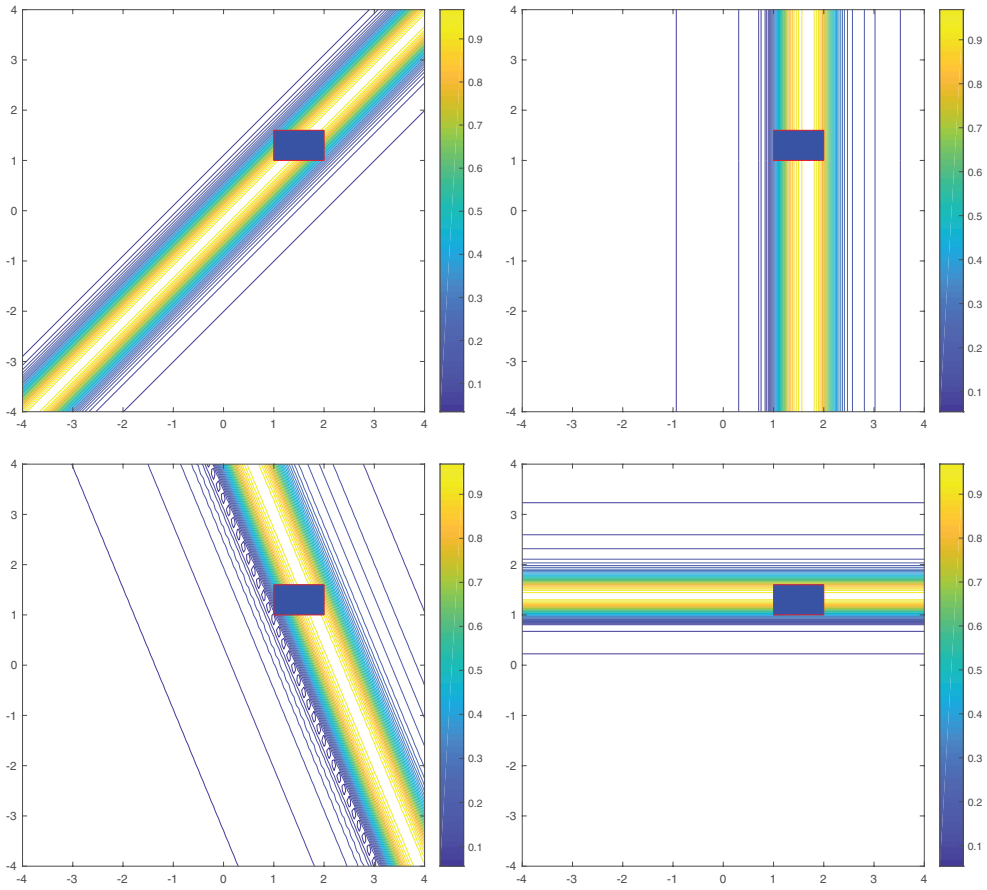

Figure 3. Reconstructions using a single observation direction for one object when $F = 5$. Top left: $\varphi = -\pi/4$. Top right: $\varphi = 0$. Bottom left: $\varphi = \pi/8$. Bottom right: $\varphi = \pi/2$.

where $N = 20$, $k_{\min} = 0.5$, $k_{\max} = 20$ such that

$$k_j := (j - 0.5)\Delta k, \quad \Delta k := \frac{k_{\max}}{N}.$$

Assume that the sampling domain is $\mathbb{S} := [-4, 4] \times [-4, 4]$. The interval $[-4, 4]$ is uniformly divided into 80 intervals and we end up with 81×81 sampling points uniformly distributed in $\mathbb{S}$. We denote by Z the set of all sampling points. We normalize the source indicator function, i.e. the plot is for $J/M(J)$ where $M(J)$ is the largest element of $J(z), z \in Z$, where $J = I^\theta$ or I. The normalized source indicator function takes the value between 0 and 1, and further can be thresholded to localize the source in practice. Since the source indicator function only involves the evaluation of a simple integral, the method is very fast in general. The Matlab code takes a few seconds for the following examples on a laptop (MacBook Pro with a 3.3 GHz Intel Core i7 processor and 16 GB memory).

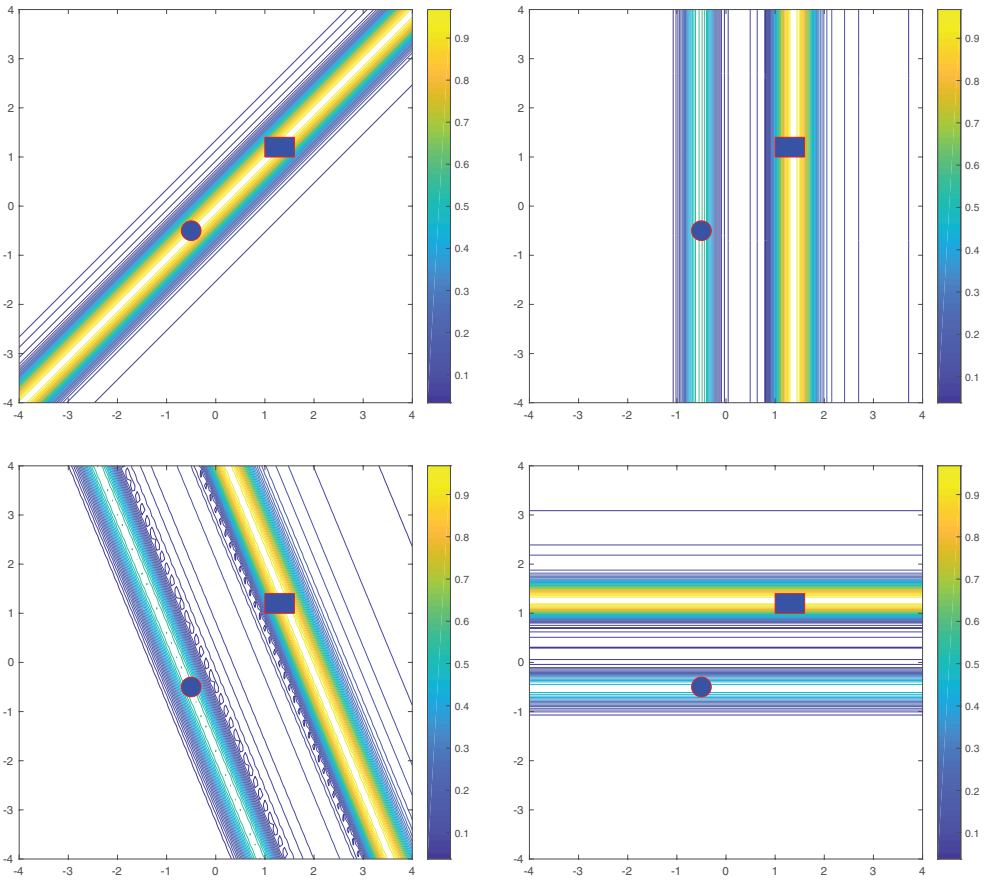

Figure 4. Reconstructions using a single observation direction for two objects when $F = 5$. Top left: $\varphi = -\pi/4$. Top right: $\varphi = 0$. Bottom left: $\varphi = \pi/8$. Bottom right: $\varphi = \pi/2$.

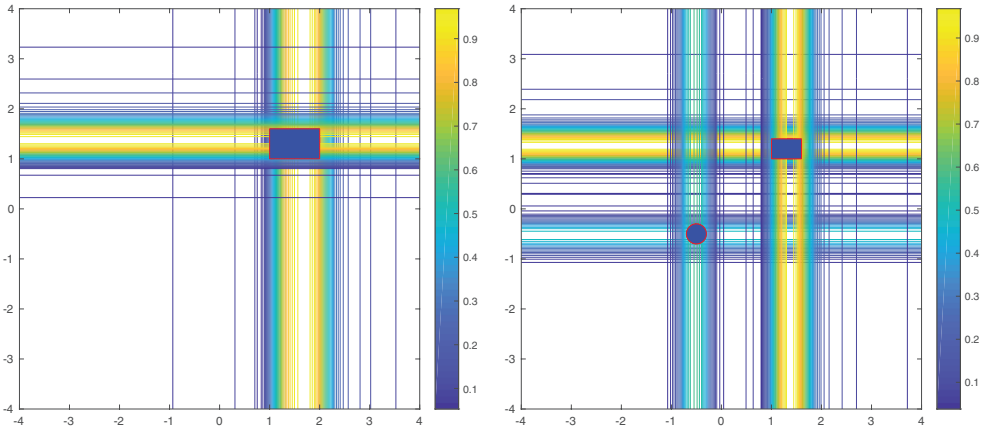

Figure 5. Reconstructions using two observation angles $\varphi = \pi/2$ and $\varphi = 0$ when $F = 5$. Left: single object; Right: two objects.

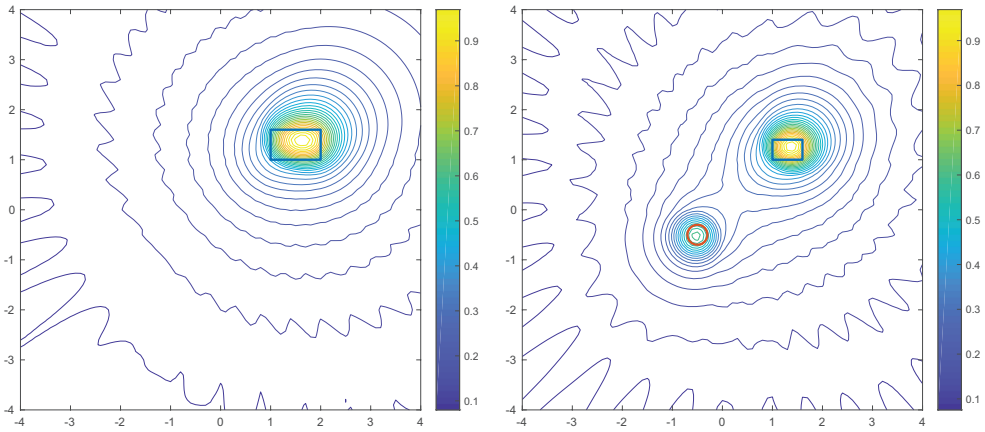

Figure 6. Reconstruction using multiple observation directions when $F = 5$. Left: single object. Right: two objects.

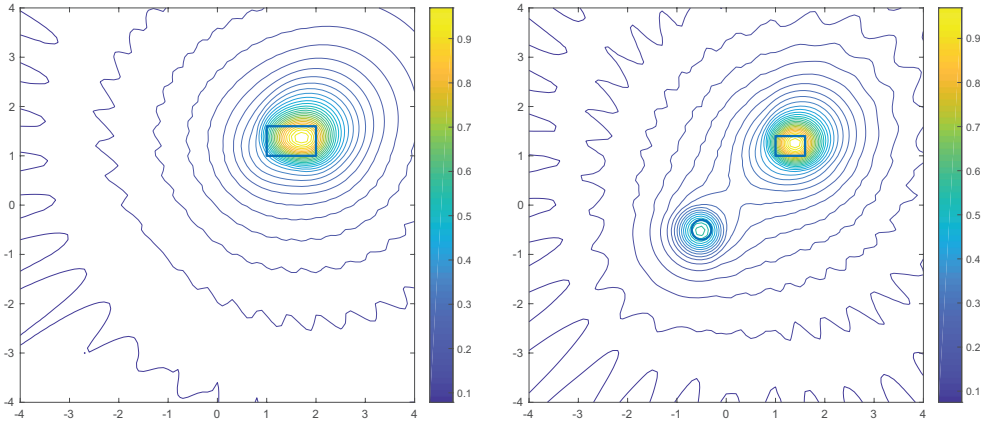

Figure 7. Reconstructions using multiple observation directions when $F(x, y) = x^2 - y^2 + 5$. Left: single object. Right: two objects.

5.1. One observation direction

We first consider the case of one observation direction $\theta \in \Theta_M$. Let $F = 5$ and the support of F is a rectangle given by $(1, 2) \times (1, 1.6)$. In figure 3, we plot the indicators for four different observation angles $\varphi = -\pi/4, 0, \pi/8$ and $\pi/2$. The picture clearly shows that the source lies in a strip perpendicular to the observation direction.

In figure 4, we show the results when the support of the source has two components. One is a rectangle given by $(1, 1.6) \times (1, 1.4)$. The other one is a disc centered at $(-0.5, -0.5)$ with radius 0.2. For different observation directions, strips containing the objects are reconstructed effectively.

5.2. Two observation directions

Now we consider two observation angles: $\varphi_1 = 0$ and $\varphi_2 = \pi/2$. We compute the indicators and superimpose them in one picture. Since the observation directions are perpendicular to

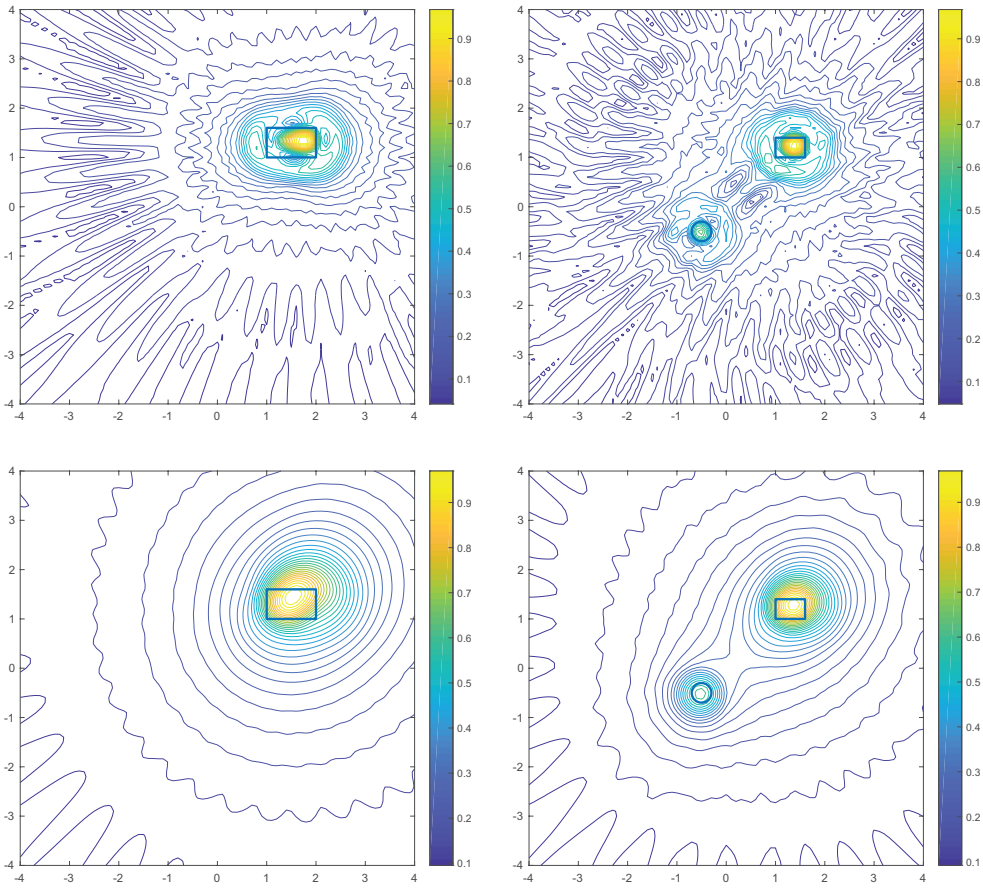

Figure 8. Reconstructions of sources depending on wave number k. Top: $F_1(x, y; k) = k^2(x^2 - y^2 + 5)$. Top left: one object. Top right: two objects. Bottom: $F_2(x, y; k) = e^{ik(x\cos 3\pi/2 + y\sin 3\pi/2)}(x^2 - y^2 + 5)$. Bottom left: one object. Bottom right: two objects.

each other, the strips are perpendicular to each other in figure 5. For both one object and two objects, we see that intersection of the strips contains the support of F.

5.3. Multiple observation directions

Now we use $M = 20$ observation angles $\varphi_j, j = 1, \ldots, 20$ such that $\varphi_j = -\pi/2 + j\pi/M$. Note that $\varphi_j \in (-\pi/2, \pi/2]$. We superimpose the indicators and show the results in figure 6. The locations and sizes of support of F are reconstructed correctly.

Next, we choose $F(x, y) = x^2 - y^2 + 5$, a function depending only on the locations. The reconstruction is shown in figure 7.

We also consider the case when the source F depends on k as well. Let

$$F_1(x, y; k) = k^2(x^2 - y^2 + 5),$$

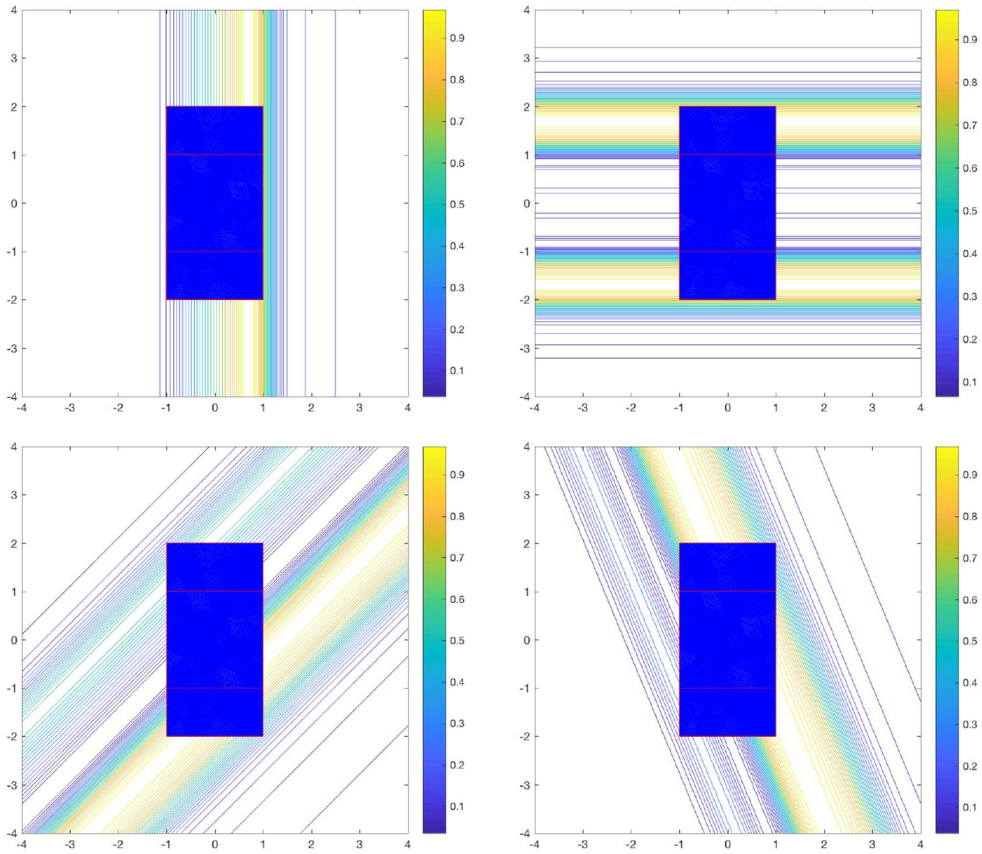

Figure 9. Reconstructions of larger object with F given in (2.11) by using a single observation direction. Top left: $\varphi = 0$. Top right: $\varphi = \pi/2$. Bottom left: $\varphi = -\pi/4$. Bottom right: $\varphi = \pi/8$.

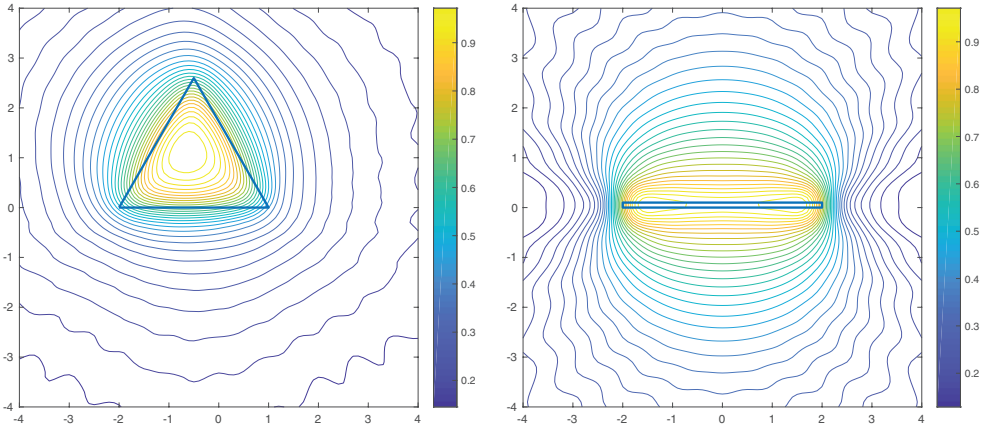

Figure 10. Reconstructions of larger objects when $F(x, y) = 5$. Left: triangle. Right: thin bar.

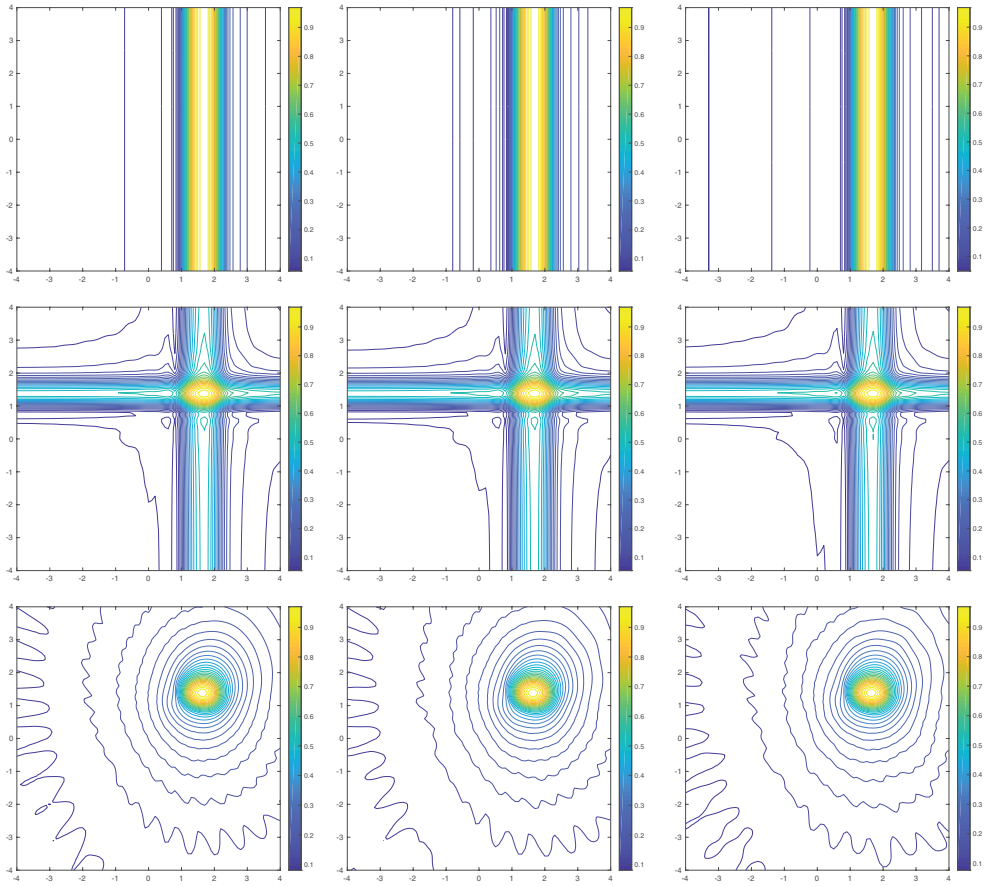

Figure 11. Contour plots of the source indicator functions with $F = 5$ and the support of F is the rectangle given by $(1, 2) \times (1, 1.6)$. Top row: one observation direction. Middle row: two observation directions. Bottom row: multiple observation directions. Left column: 10% noise. Middle column: 20% noise. Right column: 30% noise.

and

$$F_2(x, y; k) = \mathrm{e}^{\mathrm{i}k(x\cos 3\pi/2 + y\sin 3\pi/2)}(x^2 - y^2 + 5).$$

The reconstructions are shown in figure 8. Combining the previous figures 6 and 7, we observe that the reconstructions change slightly for different source functions. The location and size of the support are always well captured.

5.4. Extended objects

The sources in the above examples are small compared with the wavelengths used. Note that the smallest wavelength is $\lambda_{\min} = 2\pi/10 \approx 0.628$. In figures 9 and 10, we show the reconstructions of some larger objects. Figure 9 shows that the reconstructions of the source given in (2.11) with a single observation direction. This example further shows that theorem 2.1 does not hold in general if the set in (2.6) has positive Lebesgue measure. In fact, for observation direction $(0, 1)$, a gap appears clearly in $(-1, 1)$.

In figure 10, we show the reconstructions of two larger objects with 20 observation directions. One is an equilateral triangle with vertices

$$(-2,0), \quad (1,0), \quad (-1/2, 3/2\sqrt{3}-1).$$

The second one is a thin slab given by $(-2,2)\times(0,0.1)$. The results indicate that shorter wavelength could lead to better reconstruction. Furthermore, the shape of the support can be reconstructed as well.

5.5. Noisy Data

Finally, we show some examples using the noisy data. For simplicity, we take $F = 5$ and the support is the rectangle given by $(1,2)\times(1,1.6)$. We add 10%, 20%, and 30% normally distributed random noise to the far-field data. We show the contour plots of the source indicator functions in figure 11 for one, two, and multiple observation directions as in sections 5.1–5.3. To better see the differences, the exact rectangle is not shown. The results show that the proposed method is quite robust against random noise.

Acknowledgment

The research was supported in part by NSAF Grant (No. U1930402), NSFC Grants (No. 11671028, 11571355, 11971701) the Youth Innovation Promotion Association, CAS.

ORCID iDs

Guanghui Hu https://orcid.org/0000-0002-8485-9896
Xiaodong Liu https://orcid.org/0000-0002-3733-451X
Jiguang Sun https://orcid.org/0000-0003-4105-8463

References

[1] Bao G, Lin J and Triki F 2010 A multi-frequency inverse source problem *J. Differ. Equ.* **249** 3443–65
[2] Bao G, Lu S, Rundell W and Xu B 2015 A recursive algorithm for multi-frequency acoustic inverse source problems *SIAM J. Numer. Anal.* **53** 1608–28
[3] Colton D and Kress R 2013 *Inverse Acoustic and Electromagnetic Scattering Theory* 3rd edn (Berlin: Springer)
[4] Dassios G 2009 Electric and magnetic activity of the brain in spherical and ellipsoidal geometry *Mathematical Modeling in Biomedical Imaging I: Electrical and Ultrasound Tomographies, Anomaly Detection, and Brain Imaging* ed H Ammari (Berlin: Springer) pp 133–202
[5] Devaney A, Marengo E and Li M 2007 The inverse source problem in nonhomogeneous background media *SIAM J. Appl. Math.* **67** 1353–78
[6] Devaney A and Sherman G 1982 Nonuniqueness in inverse source and scattering problems *IEEE Trans. Antennas Propag.* **30** 1034–7
[7] El-Badia A and Ha-Duong T 2000 An inverse source problem in potential analysis *Inverse Problems* **16** 651–64
[8] El-Badia A and Ha-Duong T 2002 On an inverse source problem for the heat equation. Application to a pollution detection problem *J. Inverse Ill-Posed Problems* **10** 585–99
[9] Eller M and Valdivia N P 2009 Acoustic source identification using multiple frequency information *Inverse Problems* **25** 115005

[10] Griesmaier R and Schmiedecke C 2017 A factorization method for multi-frequency inverse source problems with spars far field measurements *SIAM J. Imaging Sci.* **10** 2119–39
[11] Hu G, Kian Y and Zhao Y 2020 Uniqueness to some inverse source problems for the wave equation in unbounded domains (arXiv:1907.02619), to appear in: Acta. Math. Appl. Sin. (a special issue on Inverse Problems in 2020)
[12] Hu G and Li J 2019 Uniqueness to time-harmonic inverse source problems with a single far-field pattern (arXiv:1907.08390)
[13] Liu X 2017 A novel sampling method for multiple multiscale targets from scattering amplitudes at a fixed frequency *Inverse Problems* **33** 085011
[14] Schuhmacher A, Hald J, Rasmussen K B and Hansen P 2003 Sound source reconstruction using inverse boundary element calculations *J. Acoust. Soc. Am.* **113** 114–27
[15] Sylvester J and Kelly J 2005 A scattering support for broadband sparse far field measurements *Inverse Problems* **21** 759–71
[16] Wang X, Guo Y, Zhang D and Liu H 2017 Fourier method for recovering acoustic sources from multi-frequency far-field data *Inverse Problems* **33** 035001